SAND2015-2891C

ILASS Americas 27th Annual Conference on Liquid Atomization and Spray Systems, Raleigh, NC, May 2015

Viscous drops impacting thin liquid surfaces: experimental quantification of secondary fragment sizes and velocities

Daniel R. Guildenbecher[*a], Carlton F. Brooks[a], and Paul E. Sojka[b]
[a]Sandia National Laboratories, Albuquerque, NM, USA
[b]School of Mechanical Engineering, Purdue University, West Lafayette, IN, USA

Abstract

The impact of liquid drops onto thin liquid films has been studied for over a century, with hundreds of papers available in the literature. However, there have been relatively few quantitative investigations of the temporal evolution of fragment properties, and, to our knowledge, all such investigations have considered water as the test liquid. This is despite the fact that more viscous liquids have been shown to dramatically alter the breakup morphology. Motivated by this, the current study presents the results of an initial investigation to quantify the temporal history of the fragments produced by the impact of viscous drops onto liquid films. Fragments are quantified using kHz digital in-line holography (DIH), which is a laser-based diagnostic discussed in a companion article (Guildenbecher, D.R., and Sojka, P.E., *ILASS Americas 27th Annual Conference on Liquid Atomization and Spray Systems*, 2015). Test liquids include pure DI water and two relatively low concentrations of carboxymethyl cellulose salt (CMC-Na) in DI water, whose measured low-shear viscosities are 4.6 and 6.4 times that of pure water. Results show that increasing viscosity (decreasing Reynolds number) at constant impact Weber number may either: (1) suppress breakup of the crown and initiate the formation of a very fine micro spray from the ejecta sheet, (2) the crown may still break up but into larger fragments compared to the inviscid case, or (3) the crown may break up into fragments which are smaller compared to the inviscid case. The exact mechanisms which produce these varied changes in fragment sizes at decreasing *Re* are not well understood, and the results are further evidence of the richness of the physics of liquid splashing. Finally, it is noted that, at sufficient concentrations, CMC-Na solutions can display shear-thinning rheology. Nevertheless, at the relatively low concentrations considered here, the observed phenomena are believe to be attributable to changes in the Newtonian dynamic viscosity.

[*]Corresponding author: drguild@sandia.gov

Introduction

The impact of drops on liquid surfaces has been widely investigated, and in the century since Worthington's initial efforts [1] hundreds of works have been published, with recent reviews given in [2-4]. Despite the large body of work and the apparent simplicity of the problem, a complete understanding of the physical processes governing droplet splashing remains elusive. For example, it was only recently theorized that more than one sheet or crown structure may be generated during impact [5], with experiments [6] confirming the presence of a fine "ejecta sheet" originating near the contact point. Later, using phase contrast x-ray imaging it was shown that once formed this ejecta sheet may either break up into a very fine spray or merge with the lamella to eventually form the well-known crown [7]. All of this indicates that, despite a hundred years of work, much remains to be learned about this fundamental multiphase flow.

In a companion article [8], we discussed a kHz digital in-line holography (DIH) methodology to quantify the sizes, three-dimensional (3D) positions, and three-component (3C) velocities of the fragments formed from the impact of a drop on a thin film. As shown in [8], a major advantage of this technique is its ability to automatically quantify a large number of fragments such that temporal size-velocity statistics can be measured. In [8], results are presented for water drops at various impact Weber numbers, $We = \rho d_0 v_0^2/\sigma$, where ρ is the liquid density, d_0 is the initial spherical diameter, v_0 is the impact velocity, and σ is the interfacial surface tension. Fragment sizes and velocities are shown to vary as a function of non-dimensional time after drop impact, $\tau = (t-t_0)v_0/d_0$, where t_0 is the impact time.

The aforementioned work is one of only a few experimental investigations of the temporal evolution of fragment sizes of which we are aware [8-10]. All of these previous works consider water as the test liquid. However, from the literature it is well-known that the impact of more viscous liquids can produce markedly different morphologies. For example, Figure 1 shows backlit high-speed images from the impact of a water drop (top row), a water drop with 0.125-wt% carboxymethyl cellulose salt (CMC-Na) (middle row), and a water drop with 0.25-wt% CMC-Na (bottom row). For all three cases, $We \approx 740$, while the Reynolds number, $Re = \rho d_0 v_0/\mu$, decreases by an order of magnitude from top to bottom. Here, μ is the dynamic viscosity. As Figure 1 clearly shows, fragmentation is a function of *We* and *Re*. Motivated by this, the current study employs DIH to reveal some unique effects of *Re* on the temporal fragment size and velocity statistics.

Beyond the Newtonian dynamic viscosity, it has also been shown that non-Newtonian effects such as visco-elasticity and shear-thinning can dramatically affect drop impact on dry surfaces [11-13]. However, to our knowledge, non-Newtonian effects have yet to be investigated for impact on liquid surfaces. Here, we choose to vary the drop viscosity using a polymer additive (CMC-Na) which can have significant shear-thinning effects. Although for the low concentrations of CMC considered in this initial investigation, it appears that the observed phenomena can be attributed to changes in the effective Newtonian viscosity. In future work, we hope to isolate any unique effects of non-Newtonian behavior by considering liquids with more pronounced non-Newtonian effects, as well as viscous Newtonian liquids.

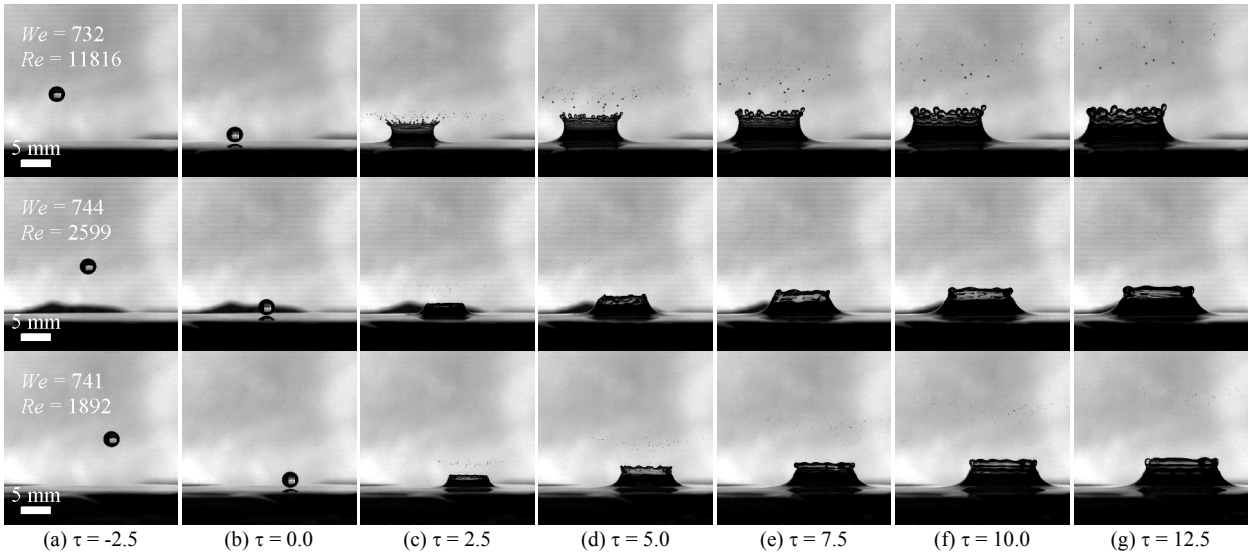

Figure 1. Select results from high-speed backlit imaging of the impact of a drop on a thin film at $We \approx 740$. Top row shows pure DI water; middle row is DI water plus 0.125-wt% CMC-Na; bottom row is DI water plus 0.25-wt% CMC-Na.

Experimental configuration

The experimental methodology for investigation of drop impact on a thin film using kHz DIH is discussed in [8]. Briefly, a collimated, frequency-doubled Nd:YAG laser beam is projected through the particle field resulting in diffraction patterns which are recorded at 20 kHz using a high-speed camera. After recording, the diffraction integral equation is used to numerically refocus the light throughout the optical depth. Image processing routines extract the 3D position of each fragment, and individual fragments are tracked over time in order to measure their velocity histories. Finally, fragments are assigned a formation time based on the start of their measured trajectory. From this, size-velocity statistics are constructed as a function of fragment formation time. Further details, including some discussion of method uncertainty, are given in [8].

Experimental liquids considered here are (1) pure DI water, (2) a mixture of 0.125-wt% CMC-Na in DI water, and (3) 0.25-wt% CMC-Na in DI water. CMC-Na is a polymer, which when added to water, is generally thought to produce an inelastic, shear-thinning fluid with viscosity described by a power law expression [14, 15]. Here, the rheology of the CMC-Na solutions was quantified using a TA Instruments AR-G2 rheometer fitted with a 60 mm diameter 2º cone operated over a nominal strain rate range of 3 to 900 s^{-1}. Over this relatively narrow strain range, the change in measured dynamic viscosity is less than 20% and fits to power-law expressions give dimensionless flow behavior indices greater than 0.966. This suggests that the fluid rheology remains essentially Newtonian at the CMC-Na concentrations considered here, although it is unknown if measurements over a larger strain rate range would lead to a different conclusion. In addition, as is discussed in the subsequent sections, drop impact behaviors observed here appear similar to previous observations using Newtonian liquids. For these reasons, results are reported here as a function of Newtonian dynamic viscosity. It is left as future work to explore a range of more non-Newtonian fluids in order to determine what effects these rheologies have on drop impact on a thin film.

Here, water is assumed to have a viscosity of 1 mPa-s. From our strain measurements, we estimate the viscosity of the 0.125- and 0.25-wt% CMC-Na solutions to be 4.6 and 6.3 mPa-s, respectively. For all solutions, the density is assumed to be that of pure water, $\rho = 1000$ kg/m^3, and the interfacial surface tension is also assumed to be that of pure water, $\sigma = 0.072$ N/m.

Experimental Results and Discussion

Table 1 summarizes the initial conditions. For each solution, two different fall heights are considered. Approximately 20 high-speed DIH videos of drop impact are recorded at each condition. From each video, the frames preceding impact are used to measure the initial drop trajectory. This gives the initial diameter, d_0, and impact velocity, v_0, from which the impact *We* and *Re* are calculated.

To begin we consider the case of the lower fall height which results in an impact $We \approx 740$. High speed backlit images of this condition are shown in Figure 1. As already discussed, these results show that the addition of even small amounts of CMC-Na can cause a dramatic effect on the flow morphology. In both the 0.125- and 0.25-wt% CMC-Na cases, a very fine spray (diameters below the single pixel resolution value of 15.8 μm) forms near the onset of impact (see column (c) at $\tau = 2.5$ in Figure 1. Note the fine spray is barely distinguishable at this magnification). In addition, the higher viscosity CMC-Na solutions suppress the growth of the crown and prevent any pinch-off of fragments from the crown. Similar results have been previously observed for Newtonian liquids, such as the glycerol/water solution in Zhang *et al.* [16] at $We = 314$, $Re = 2566$. This leads us to believe that the observed phenomena are likely due to Newtonian viscous effects.

In [16, 17] a morphological map is proposed for the transition between "crown splash and micro-droplet splash", such as shown in the top row of Figure 1, and "micro-droplet splash" alone as shown in the bottom two rows. That map predicts that below a certain *We*, decreasing *Re* leads to suppression of the crown splash. Our results generally agree with these trends. Note, in [16, 17] micro-droplet splash is observed for $We \lesssim 500$. Here micro-droplet splash is observed for *We* as high as 750. The discrepancy in the transition *We* may be due to differences in dimensionless film thickness ($\delta = h/d_0 = 0.2$ in [16, 17] and $\delta = 0.9$ here).

Table 1. Initial conditions, given as the mean from all videos ± the standard deviation of the mean from each video.

wt% CMC-Na	Approximate fall height (mm)	Number of videos analyzed	Initial diameter, d_0 (mm)	Impact velocity, v_0 (m/s)	Dimensionless film thickness, δ	Impact Weber number, *We*	Impact Reynolds number, *Re*
0.00	1250	13	2.645 ± 0.009	4.48 ± 0.01	0.889 ± 0.003	737 ± 6	11849 ± 61
0.00	2250	20	2.648 ± 0.006	5.62 ± 0.02	0.888 ± 0.002	1160 ± 10	14875 ± 74
0.125	1250	20	2.667 ± 0.005	4.48 ± 0.02	0.881 ± 0.002	744 ± 5	2599 ± 10
0.125	2250	20	2.647 ± 0.005	5.62 ± 0.02	0.888 ± 0.002	1160 ± 9	3232 ± 13
0.25	1250	20	2.665 ± 0.012	4.49 ± 0.02	0.881 ± 0.004	744 ± 8	1897 ± 13
0.25	2250	22	2.648 ± 0.005	5.61 ± 0.02	0.888 ± 0.002	1156 ± 8	2357 ± 9

To investigate the formation of this micro-droplet splash in more detail, Figure 2 shows select DIH results at early times ($\tau \leq 1$). These images are found by numerically refocusing the digital hologram to the plane of impact, z_0. To highlight the behavior near the impact point, the images are magnified and cropped from the total *x*-*y* extent of the hologram. The dark black structures are the drop and film, while the light gray rings are the out-of-focus twin-images [18, 19]. These results demonstrate the advantage of DIH to refocus and observe fine flow structures, which are not always captured in-focus in traditional white light images such as Figure 1.

These results can be understood via comparison to the phase contrast x-ray images provided in [7]. At lower *Re*, the more viscous solutions display a distinct ejecta sheet, which emanates radially from the point of impact, and a separate lamella, which evolves into the crown. The ejecta sheet breaks up to form a fine micro spray with droplet sizes approaching the effective pixel size (15.8 μm). In contrast, for the nearly inviscid water case no distinct ejecta sheet is observed. Rather, if an ejecta sheet has formed, it merged with the lamella to form the crown in a time less than 120 μsec.

In many spray processes, increased viscosity slows liquid deformation and increases secondary fragment sizes (for example refer to the many empirical atomization performance relations given in Lefebvre's book [20]). In contrast, Figure 2 indicates that under certain conditions, increased viscosity may decrease the mean size of fragments produced from the impact of a drop on a liquid film. To further investigate this, Figure 3 shows the evolution of drop impact at later times ($2.5 \leq \tau \leq 12.5$). Here, each row is taken from the identical impact events shown at earlier times in Figure 2. In addition, the results in Figure 3 are overlaid with the measured in-plane fragment sizes (colored circles) and velocity vectors. These results qualitatively show that at high *Re*, fragments produced from the crown have a mean size well above the size detection limit of the DIH system (~40 μm). However, at lower *Re*, many fragments are below the size detection limit and are not measured. Interestingly, as *Re* decreases from the middle to bottom row, comparatively more micro-drops are measured. This is qualitative evidence that fragments which are produced from the ejecta sheet do show the expected increase in mean sizes with increasing viscosity. In summary, we can hypothesize that fragments produced from a single mechanism (e.g. ejecta sheet fragments or crown fragments) show increasing mean diameters with increasing viscosity. However, because multiple fragment production mechanisms are possible and viscous effects may suppress one or more of these mechanisms, viscous effects may lead to unexpected changes in overall mean fragment sizes (such as when the crown drop formation mechanism vanishes).

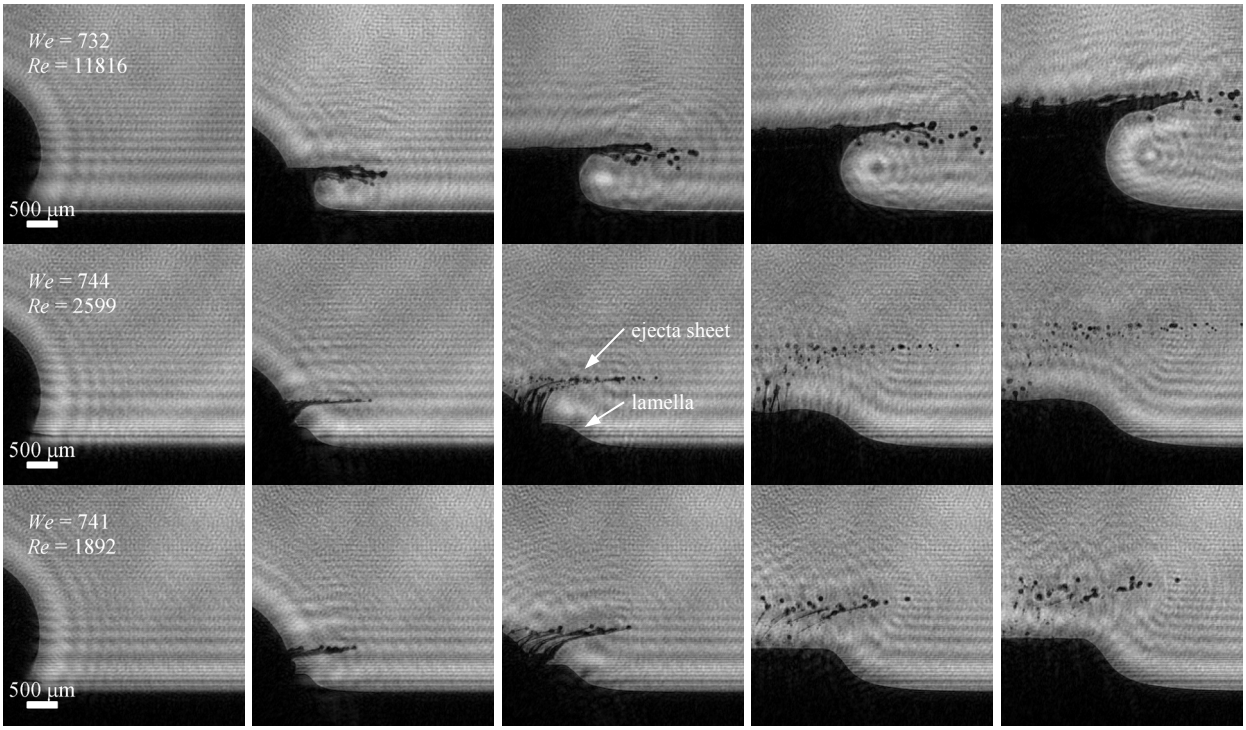

(a) $\tau = 0.2$ (b) $\tau = 0.4$ (c) $\tau = 0.6$ (d) $\tau = 0.8$ (e) $\tau = 1.0$

Figure 2. Selected DIH results from early times after impact of a drop on a thin film at $We \approx 740$. Top row shows pure DI water; middle row is 0.125-wt% CMC-Na in DI water; bottom row is 0.25-wt% CMC-Na in DI water.

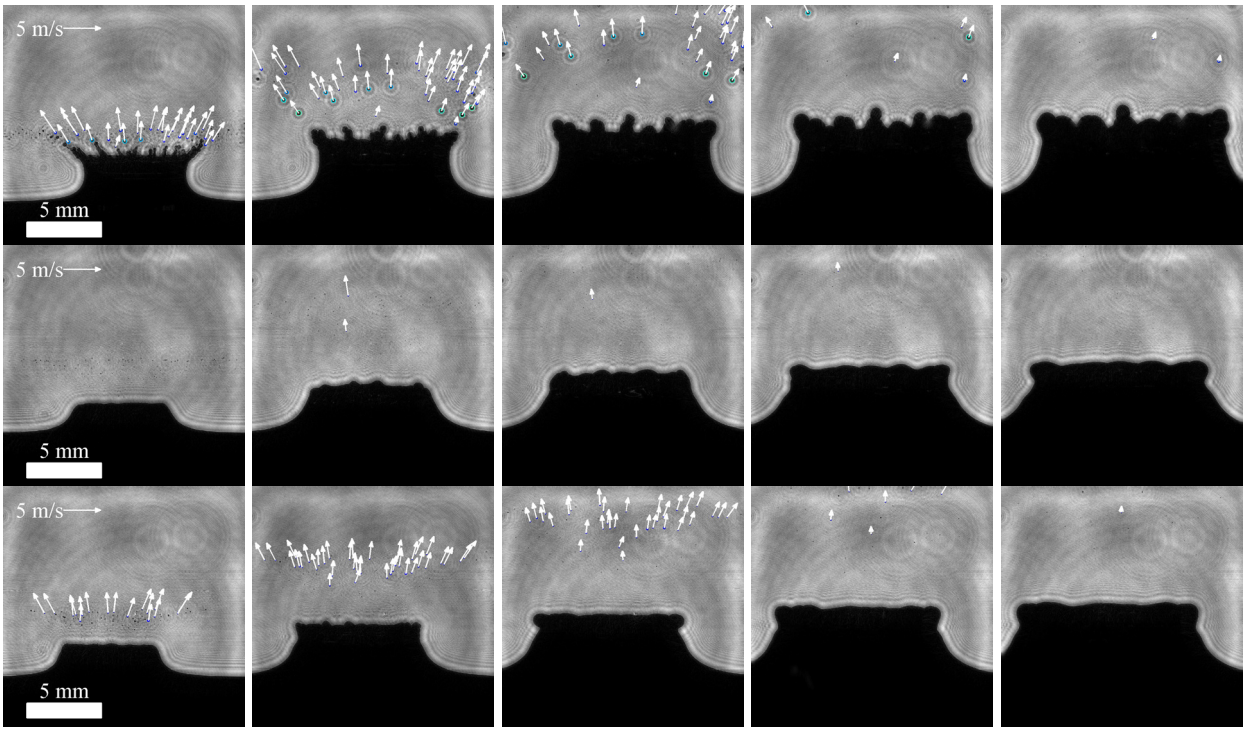

(a) $\tau = 2.5$ (b) $\tau = 5.0$ (c) $\tau = 7.5$ (d) $\tau = 10.0$ (e) $\tau = 12.5$

Figure 3. Selected DIH results from late times after impact of a drop on a thin film at $We \approx 740$. Top row shows pure DI water; middle row is 0.125-wt% CMC-Na in DI water; bottom row is 0.25-wt% CMC-Na in DI water.

Note that with higher magnification it should be possible to quantify a majority of the micro-droplet fragments, whose mean size is thought to be on the order of a few 10s of μm [7]. For example, in [21, 22] we employ magnified DIH configurations to quantify particles sizes down to approximately 10 μm. This is left for future work, and for the time being we purposely omit here any quantitative measured of mean fragments sizes at $We \approx 740$ and low *Re*, as these results are likely to be highly biased by the current size detection limit of 40 μm. Quantitative results on the breakup of the water drop at $We \approx 740$ can be found in [8].

We now consider the case of the larger fall height which results in an impact $We \approx 1160$. Figure 4 and Figure 5 present select DIH results in an analogous manner to the results presented in Figure 2 and Figure 3, respectively. In Figure 4 a micro spray is observed to emerge almost immediately after impact for pure water at the intermediate *Re*. The source of this micro spray is presumed to be breakup of the ejecta sheet. Once again, the size of these fragments is below the size detection limit of the current DIH configuration.

At the lowest *Re*, viscous effects appear to suppress the micro spray, and the ejecta sheet (if present) must have already merged with the crown. This is consistent with the observations of Deegan *et al*. [17] and Zhang *et al*. [16] who report that at high *We*, decreasing *Re* eventually suppresses the micro spray. (Note that [7, 17] refer to a "crown and micro-droplet splash morphology". The top two rows in Figure 4 clearly fall into this category while the bottom row may or may not depending on interpretation of this morphology. Nevertheless, the conclusion that decreasing *Re* at high *We* leads to suppression of the micro spray is consistent.)

Finally, and perhaps more interestingly, Figure 5 qualitatively shows that decreasing *Re* initially leads to a decrease in the number of fragments and an increase in the fragment size when compared to the DI water case. However, at the highest concentration of CMC-Na, the number of fragments once again increases, while the mean fragment size decreases. This is quantified in Table 2 which reports selected mean diameters for all fragments measured at each of the three conditions.

A complete explanation for this inconsistent change in mean fragment sizes as a function of *Re* is not yet known. Perhaps the ejecta sheet, which may have merged with the crown at low *Re*, contributes to the production of a relatively large number of small fragments at around $\tau = 2.5$. These results are further evidence that viscous effects can produce surprising changes in the mean fragment sizes. Note that this is despite the fact that no distinct change in breakup morphology is observed, unlike the results at $We \approx 740$.

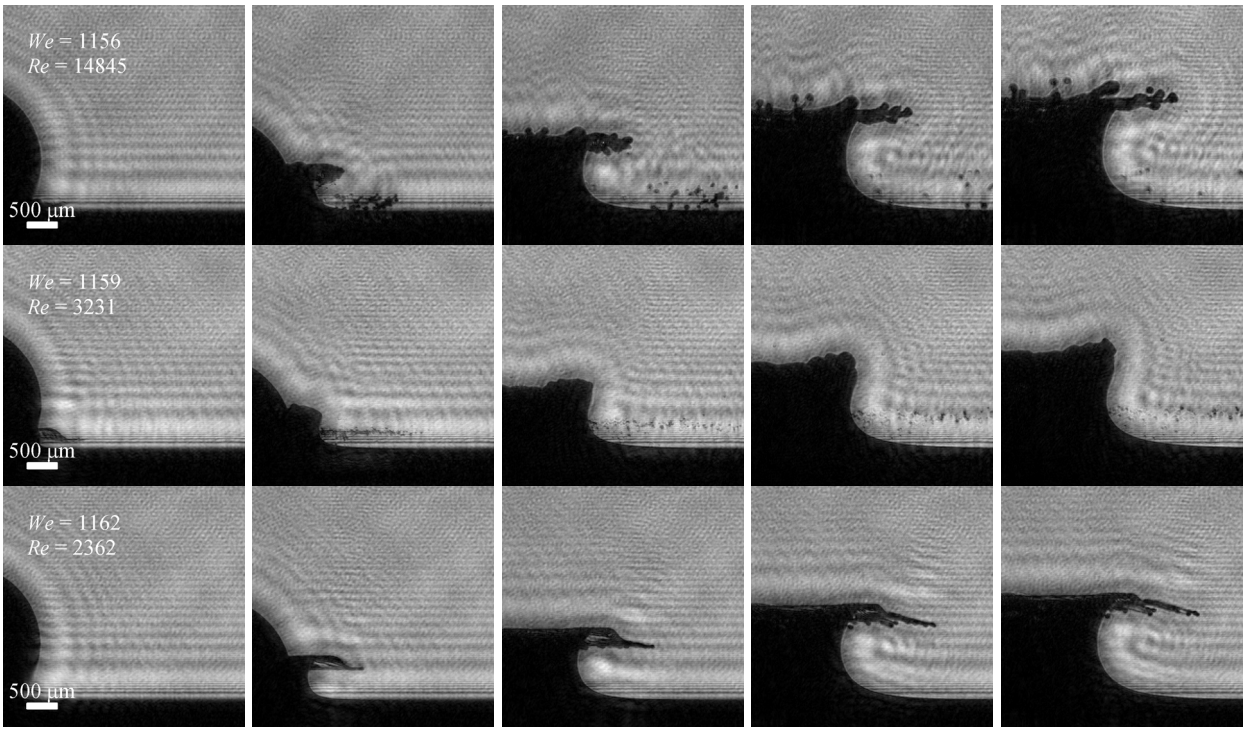

(a) τ = 0.2 (b) τ = 0.4 (c) τ = 0.6 (d) τ = 0.8 (e) τ = 1.0

Figure 4. Selected DIH results from early times after impact of a drop on a thin film at *We* ≈ 1160. Top row shows pure DI water; middle row is 0.125-wt% CMC-Na in DI water; bottom row is 0.25-wt% CMC-Na in DI water.

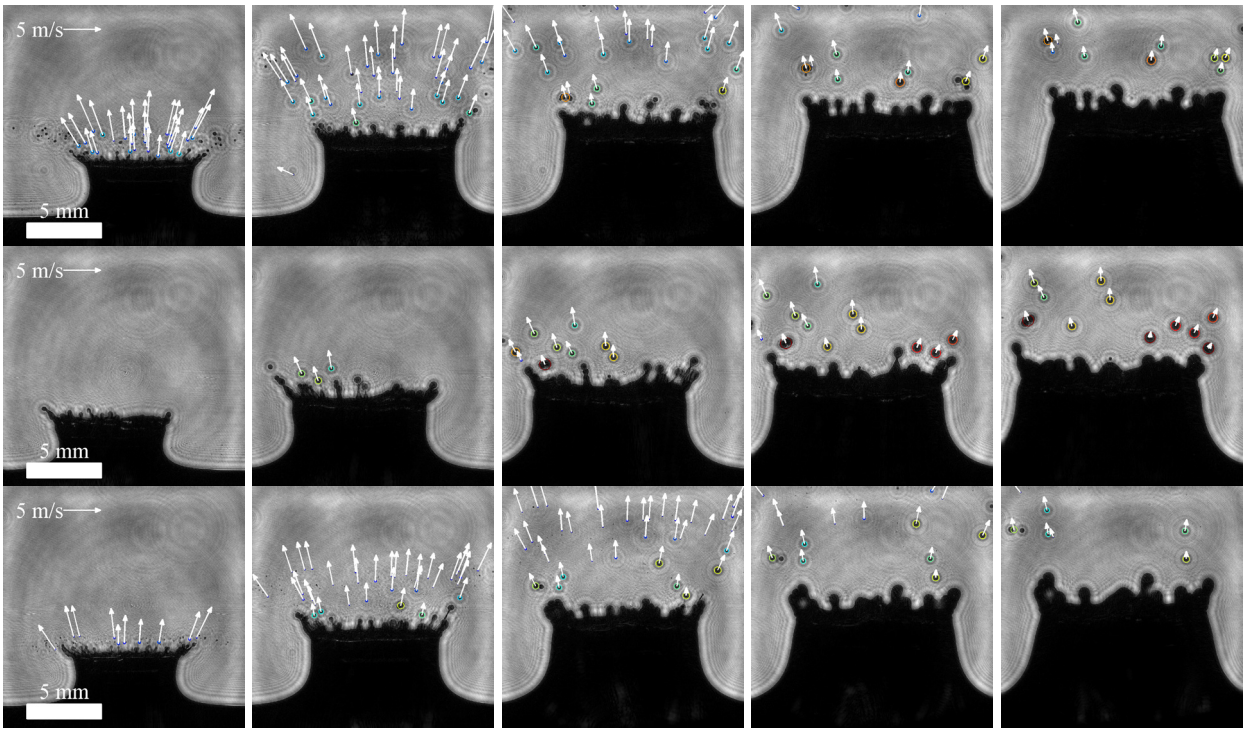

(a) τ = 2.5 (b) τ = 5.0 (c) τ = 7.5 (d) τ = 10.0 (e) τ = 12.5

Figure 5. Selected DIH results from late times after impact of a drop on a thin film at *We* ≈ 1160. Top row shows pure water; middle row is 0.125 wt% CMC-Na in water; bottom row is 0.25 wt% CMC-Na in water.

Table 2. Characteristic sizes of the fragments for $We \approx 1160$, given as the mean from all videos ± the standard deviation of the mean from each video.

wt% CMC -Na	Number of measured fragments	D_{10} (μm)	D_{30} (μm)	D_{32} (μm)
0.00	59 ± 6	209 ± 17	286 ± 20	382 ± 42
0.125	32 ± 14	251 ± 108	330 ± 108	423 ± 104
0.25	41 ± 7	138 ± 30	248 ± 58	422 ± 108

These results are further summarized in Figure 6 and Figure 7 which show the measured number of fragments and fragment size-velocity statistics, respectively, as a function of estimated fragment production time. An explanation of the methods used to calculate these figures can be found in [8].

Figure 6 confirms what was qualitatively observed in Figure 5. That is, as CMC-Na concentration increases, fragment production initially decreases and then increases again at the highest CMC-Na concentration.

Figure 7(a) shows the mean fragment sizes as a function of production time. Again, this quantifies the trends which are qualitatively observed in Figure 5.

Finally, Figure 7(b)-(c) show mean fragment velocities as a function of producton time. Interestingly, at the highest CMC-Na concentration, the measured radial velocities are signifigantly different. However, in Figure 5 the radial growth of the crown appears qualitatively similar for all cases. This indicates that, at least for some conditions, models of the crown radial velocity (e.g., Yarin [23]) may be insufficient to predict fragment radial velocities.

Summary and Conclusions

The work presented here employs kHz digital in-line holography (DIH) to investigate the fragments produced from the impact of inviscid and viscous drops on thin films. The liquids considered include pure DI water and mixtures of 0.125- and 0.25-wt% carboxymethyl cellulose (CMC-Na) in DI water, whose measured low-shear viscosity is roughly 4.6 and 6.3 times that of pure DI water, respectively. As the Reynolds number is decreased at constant Weber number several phenomena are observed: they are either (1) crown formation is suppressed while the ejecta sheet breaks up into a micro spray of fragments whose sizes are below the system resolution of 15.8 μm, (2) the crown breaks up into larger fragments compared to the inviscid case by a mechanism such as the one proposed by Yarin and Weiss [23], or (3) the crown breaks up into fragments which are smaller than the inviscid case via a mechanism which is not well understood. The results therefore indicate that viscous effects may produce unexpected changes to the mean fragment sizes and are further evidence of the richness of the physics of liquid splashing.

Finally, it is acknowledged that mixtures of CMC-Na and water can show significant non-Newtonian rheology when sufficient concentrations are used. At the relatively low concentrations of CMC-Na considered here, non-Newtonian effects are thought to be minimal (the power-law flow behavior index, n, is above 0.966). However, it remains possible that some of the observed phenomena should be attributed to shear-thinning behavior. In future work, we hope to isolate any unique effects of non-Newtonian behavior by considering liquids with more pronounced non-Newtonian effects, as well as a larger range of viscous Newtonian liquids.

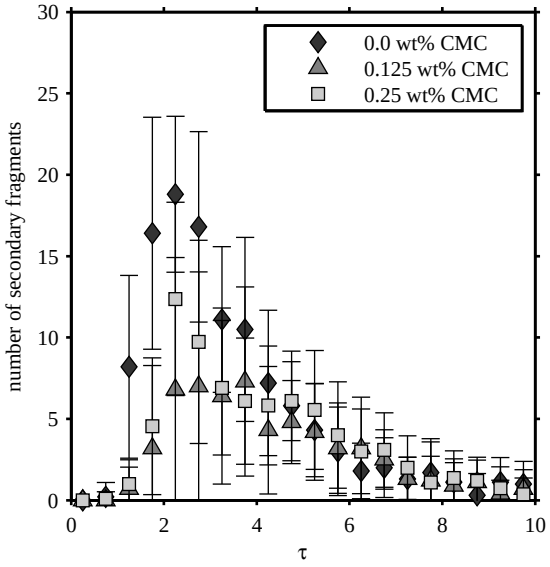

Figure 6. Measured number of secondary fragments for $We \approx 1160$ and three concentration of CMC-Na in water.

Acknowledgements

This work was supported by the Weapons Systems Engineering Assessment Technology program, and the Laboratory Directed Research and Development program at Sandia National Laboratories which is a multiprogram laboratory operated by Sandia Corporation, a Lockheed Martin Company, for the United States Department of Energy's National Nuclear Security Administration under contract No. DE-AC04-94AL85000.

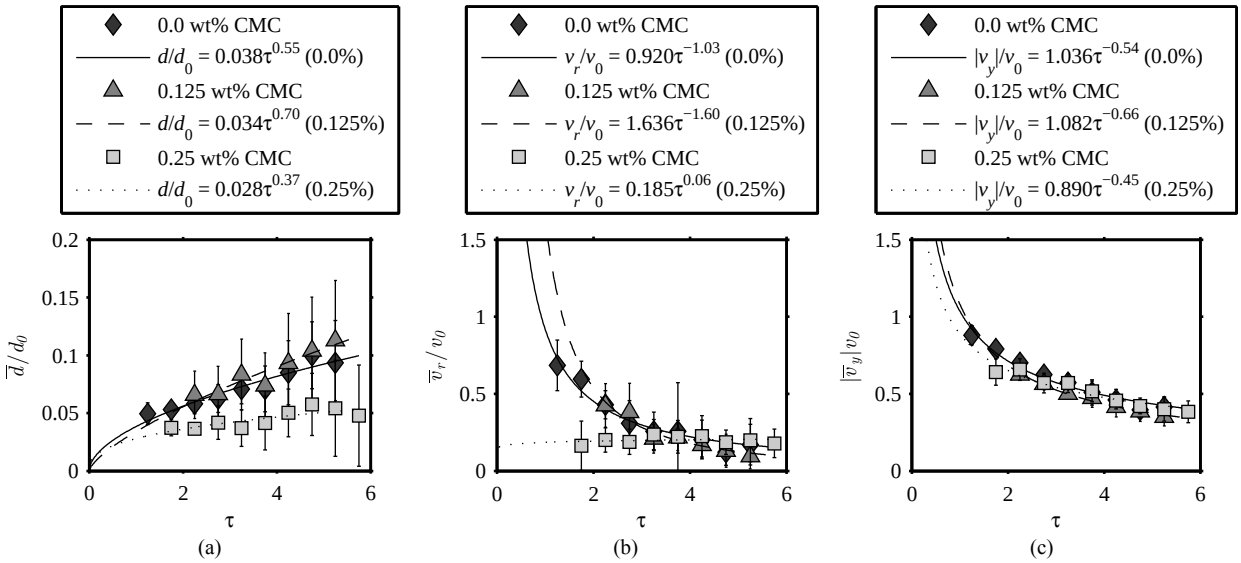

Figure 7. Comparison of (a) measured fragment sizes, (b) measured fragment radial velocities, and (c) measured fragment *y*-velocities at $We \approx 1160$.

References

[1] Worthington, A.M., *A Study of Splashes*, Longmans, Green, and Company, 1908.

[2] Yarin, A.L., *Annual Review of Fluid Mechanics*, 38(1): 159-192, (2006).

[3] Thoroddsen, S.T., Etoh, T.G., and Takehara, K., *Annual Review of Fluid Mechanics*, 40: 257-285, (2008).

[4] Moreira, A.L.N., Moita, A.S., and Panão, M.R., *Progress in Energy and Combustion Science*, 36(5): 554-580, (2010).

[5] Weiss, D.A., and Yarin, A.L., *Journal of Fluid Mechanics*, 385: 229-254, (1999).

[6] Thoroddsen, S.T., *Journal of Fluid Mechanics*, 451: 373-381, (2002).

[7] Zhang, L.V., Toole, J., Fezzaa, K., and Deegan, R.D., *Journal of Fluid Mechanics*, 690: 5-15, (2012).

[8] Guildenbecher, D.R., and Sojka, P.E., *ILASS Americas 27th Annual Conference on Liquid Atomization and Spray Systems*, 2015.

[9] Cossali, G.E., Marengo, M., Coghe, A., and Zhdanov, S., *Experiments in Fluids*, 36(6): 888-900, (2004).

[10] Guildenbecher, D.R., Engvall, L., Gao, J., Grasser, T.W., Reu, P.L., and Chen, J., *Experiments in Fluids*, 55: 1670, (2014).

[11] Bergeron, V., Bonn, D., Martin, J.Y., and Vovelle, L., *Nature*, 405(6788): 772-775, (2000).

[12] Rozhkov, A., Prunet-Foch, B., and Vignes-Adler, M., *Journal of Non-Newtonian Fluid Mechanics*, 134(1–3): 44-55, (2006).

[13] Moita, A.S., Herrmann, D., and Moreira, A.L.N., *Applied Thermal Engineering* (2014).

[14] Savvas, T.A., Markatos, N.C., and Papaspyrides, C.D., *Applied Mathematical Modelling*, 18(1): 14-22, (1994).

[15] Kaur, N., Singh, R., and Wanchoo, R.K., *Transport in Porous Media*, 90(2): 655-671, (2011).

[16] Zhang, L.V., Brunet, P., Eggers, J., and Deegan, R.D., *Physics of Fluids*, 22(12): 122105, (2010).

[17] Deegan, R.D., Brunet, P., and Eggers, J., *Nonlinearity*, 21(1): C1, (2008).

[18] Schnars, U., and Jueptner, W., *Digital holography: Digital hologram recording, numerical reconstruction, and related techniques*, Springer, 2005.

[19] Katz, J., and Sheng, J., *Annual Review of Fluid Mechanics*, 42: 531-555, (2010).

[20] Lefebvre, A.H., *Atomization and Sprays*, Hemisphere Pub. Corp., 1989.

[21] Gao, J., Guildenbecher, D.R., Reu, P.L., Kulkarni, V., Sojka, P.E., and Chen, J., *Optics Letters*, 38(11): 1893-1895, (2013).

[22] Guildenbecher, D.R., Cooper, M.A., Gill, W., Stauffacher, H.L., Oliver, M.S., and Grasser, T.W., *Optics Letters*, 39(17): 5126-5129, (2014).

[23] Yarin, A.L., and Weiss, D.A., *Journal of Fluid Mechanics*, 283: 141-173, (1995).